

Ferroelectricity and topological vortices from molecular ordering in metal-organic frameworks

Francesco Foggetti,^{1,2} Alessandro Stroppa,³ and Sergey Artyukhin¹

¹*Quantum Materials Theory, Italian Institute of Technology, Via Morego 30, 16163 Genova, Italy*

²*Department of Physics, University of Genova, Via Dodecaneso, 33, 16146 Genova GE*

³*Consiglio Nazionale delle Ricerche, Institute for Superconducting and Innovative Materials and Devices (CNR-SPIN),
c/o Department of Physical and Chemical Sciences,
University of L'Aquila, Via Vetoio, I-67100, Coppito, L'Aquila, Italy*

Metal-organic frameworks comprehend a wide class of hybrid organic-inorganic materials with general structure A_mBX_n , with A and X being organic molecules and B a metal cation. This often results in enhanced structural flexibility and new functionalities. Hybrid perovskites ABX_3 are a well-known example. In an Iron-based perovskites, $(\text{DMA})\text{Fe}^{II-III}(\text{COOH})_3$, dimethylammonium (DMA) molecules are organized in a hexagonal structure [1]. They are orientationally disordered at high temperatures, but order at around $T = 100$ K in a peculiar toroidal pattern. Recent experimental and theoretical study suggest the appearance of ferroelectric polarization in this phase, although the measured polarization is small, and the mechanism of ferroelectricity is still debated. We formulate a Landau-type theory that clarifies the connection between the electric polarization, molecular pattern, and distortive modes of the inorganic lattice. We find a remarkable mechanism of improper ferroelectricity, analogue to the trimerization process in inorganic hexagonal ferrites and manganites, but here driven by the ordering of organic molecules in a metal-organic framework. Our study reveals an extremely rich phase diagram with the prediction of topological domain walls, where the ferroelectricity arise from tripling the unit cells due to molecular ordering. Wide domain walls with inner structure are predicted.

Introduction – Metal-organic frameworks (MOFs) are hybrid organic-inorganic compounds where the presence of organic molecules enables novel properties, not replicated by any inorganic-based compounds [2] and resulting in cheaper materials with superior performance or new functionalities. Despite many molecules are polar, observations of ferroelectricity in molecular compounds has been limited until recently [3, 4]. New mechanisms, specific for organic compounds, have been identified, including neutral-to-ionic transition in charge transfer complexes, and hydrogen bond mechanism, as realized in donor-acceptor molecular chain compounds [5]. Co-DMA metal-organic framework, involving dimethylammonium (DMA) molecules $\text{NH}_2(\text{CH}_3)_2$, has recently been discovered to host multiferroic state [6]. The hybrid nature may combine the advantages of both organic and inorganic semiconductors for optoelectronic applications. For example, a striking and very recent direction is the possibility to exploit the chirality of the organic component for obtaining chiral hybrid perovskites through the transfer of the chirality of the molecules to the achiral octahedral layers.[7]

A peculiar MOF is $(\text{DMA})\text{Fe}^{II-III}(\text{COOH})_3$, a mixed-iron hybrid inorganic-organic perovskite. *Ab-initio* calculations suggested a polar structure below 100 K with $R3c$ space group [8]. In this phase, DMA molecules order and the estimated ferroelectric polarization along (111) direction is ~ 7 nC/cm², slightly larger than the experimental measured polarization about 1 nC/cm² [9].

However, due to the complexity and size of the system, the exact origin of ferroelectricity has not been

clearly identified. It may be related to molecular orientations or charge order. Moreover, ferroelectric order of molecules with magnetic ordering of Fe ions, could lead to a multiferroic state [6]. Here, we build a phenomenological modeling based on symmetry considerations in order to address the microscopic origin of ferroelectricity in $(\text{DMA})\text{Fe}^{II-III}(\text{COOH})_3$ and to study possible topological defects.

This paper proceeds as follows: the polar $R3c$ structure is considered as a starting point, we then introduce a parent structure and all possible displacive modes that are responsible for the transition to the polar structure. The identified modes act as order parameters for the transition between high and low symmetry structures. Finally a symmetry analysis of the low symmetry structure is performed and a Landau free energy is built from possible low-order invariants. This allows us to model the interactions between molecular orientation pattern and ferroelectricity. We find a region of model parameters where material behaves as improper ferroelectric, with the polarization originating from toroidal molecular order. We also predict 3 or 6-fold vortex topological defects, as suggested by the form of the free energy.

Symmetry considerations – Our analysis of the system starts with the low-symmetry structure having the polar space group $R3c$ (#161 in the International Tables)[10]. The symmetry breaking at low temperatures is due to the ordering on the DMA molecules in a toroidal pattern, and the associated displacements of the neighboring ions, illustrated in Fig. 1(c). We thus identify the higher symmetry structure by removing the DMA molecules and looking only at the distortions of the framework. Very

recently, Fe-MOF was suggested to have an antiferroelectric state at low T [10], while indications of ferroelectricity were observed [9] and theoretical predicted [8]. We will see below, that our microscopic model can explain this contradictory results.

We search for pseudosymmetry parent groups using Pseudosymmetry Utility of the Bilbao Crystallographic Server [11] and by sequentially removing trimerizing mode P_2 and ferroelectric displacements Γ_2^- , we find a candidate parent structure with space group $P\bar{3}_1c$ (#163 in the International Tables, Fig. 1(b)). Incidentally, we note that this structure has also been observed experimentally [10]. By performing mode decomposition [12, 13] of the low-temperature structure, where the DMA molecules have been removed, with respect to this parent structure, we find the P_2 and a polar Γ_2^- modes with amplitudes of 2.32 Å and 0.15 Å respectively. P_2 mode describes modulated displacements of $(\text{COOH})^-$ organic ligands due to rotating molecular pattern in the original structure, while ferroelectric Γ_2^- mode corresponds to polar ionic shifts along the c axis. Fig. 1(b) describes how these modes break the symmetry of the parent structure and bring the system into the lower symmetry phase. Table I shows all possible invariant quantities that we build with P_2 and Γ_2^- modes, up to the 6th order.

Model – We use the mode amplitudes for Γ_2^- and P_2 modes as order parameters to construct a Landau-type free energy of the system,

$$F = \gamma P_z^2 + (-AQ^2 - BQ^4 + CQ^6) + \alpha Q^3 \sin 3\phi + \eta Q^6 \sin^2 3\phi + V(P_z, Q, \phi), \quad (1)$$

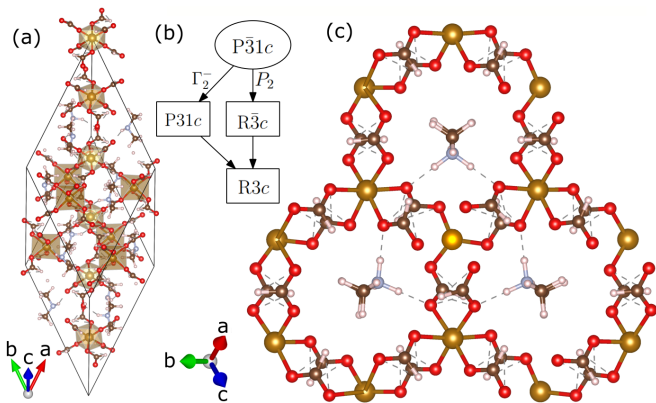


FIG. 1. (a) Rhombohedral unit cell of $(\text{DMA})\text{Fe}^{II-III}(\text{COOH})_3$ in space group $P\bar{3}_1c$. Fe ions are indicated by light brown balls and oxygens are in red. (b) Symmetry lowering paths, corresponding to different orders in which distortions are removed during the pseudosymmetry search, and the corresponding space groups. The toroidal ordering of molecules (P_2 mode) (c) View on the slice of the Fe-MOF along the (111) polar direction. DMA molecules reside in circular voids and order in a toroidal fashion. Hydrogen bonds are indicated by dashed lines.

Degree	Invariants
2	$Q_x^2 + Q_y^2, P_z^2$
3	$3Q_x^2 Q_y - Q_y^3$
4	$P_z^4, Q_x^4 + 2Q_x^2 Q_y^2 + Q_y^4$ $P_z^2(Q_x^2 + Q_y^2), P_z(Q_x^3 - 3Q_x Q_y^2)$
6	$(3Q_x^2 Q_y - Q_y^3)^2, P_z^6, P_z^4(Q_x^2 + Q_y^2),$ $P_z^2(Q_x^2 + Q_y^2)^2, (Q_x^2 + Q_y^2)^3,$ $P_z^3(Q_x^3 - 3Q_x Q_y^2), P_z(Q_x^2 + Q_y^2)(Q_x^3 - 3Q_x Q_y^2)$

TABLE I. Invariants for symmetry group $P\bar{3}_1c$ (# 163). Q_x and Q_y are the components of the P_2 mode while P_z refers to Γ_2^- mode.

with $\mathbf{Q} = (Q_x, Q_y) = (Q \cos \phi, Q \sin \phi)$ parametrizing the P_2 mode and P_z standing for the ferroelectric polarization induced by Γ_2^- mode. P_z is bounded to be small close to the phase transition, therefore we neglect high order terms in P_z from Table I. The term $V(P_z, Q, \phi)$ describes the coupling between the distortive mode and the ferroelectric polarization. The term with $\gamma > 0$ describes a stable polar mode with ferroelectric polarization P_z , while the term in parentheses represents a Mexican hat potential. The terms with α and η produce a triangular warping of the rim of the Mexican hat, generating three degenerate minima similar to those in Fig. 2(c,c'). These terms take into account the 3-fold symmetric anisotropy and are related to the symmetry of the framework that contains the molecules. Microscopically, these terms correspond to the anisotropy energy of the molecule, i.e. to the energy cost of 60° rotation away from the easy direction. The terms with α and η result from interactions between the molecule and neighboring ions, cf. Fig. 1(c). The interaction between the polarization P_z and the Q mode is given by the term

$$V(P_z, Q, \phi) = \beta P_z(Q_x^3 - 3Q_x Q_y^2) = \beta P_z Q^3 \cos 3\phi, \quad (2)$$

that is another invariant shown in Table I. In principle a term $P_z Q^5 \cos 3\phi$ should also be considered, but Q is small close to the phase transition and the cosine term is the same as the 3rd order term, therefore this term does not change the angular structure of the minima and, therefore, it can be neglected. We observe that polarization changes sign under 60° rotation of the vector \mathbf{Q} , i.e. a rotation of all the molecules by 60°.

We now minimize the free energy F with respect to P_z , which gives

$$P_z|_{min} = -\frac{\beta Q^3}{2\gamma} \cos 3\phi, \quad (3)$$

and at this optimal P_z the free energy is

$$F = -\frac{\beta^2 Q^6}{4\gamma} \cos^2 3\phi + \alpha Q^3 \sin 3\phi + \eta Q^6 \sin^2 3\phi - AQ^2 - BQ^4 + CQ^6. \quad (4)$$

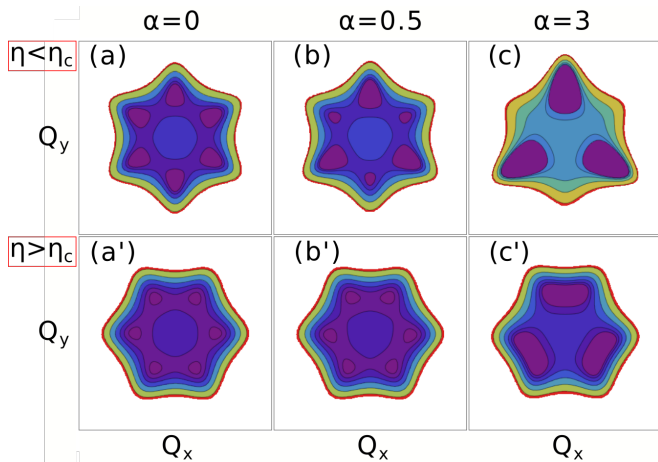


FIG. 2. Different energy densities for different values of α and η . (a-c) $\eta < \eta_c$ case. (a) In $\alpha = 0$ there are six equivalent minima, (b) three minima become less deep until they become maxima (c) for the free energy. (a'-c') $\eta > \eta_c$ case. (a') in $\alpha = 0$ six minima are present, the angular position of the minima is rotated with respect to the (a) case due to the $\eta \sin^2 3\phi$ term dominating over the $\cos^2 3\phi$. (b') the position of the minima changes, deforming the structure, pair of minima start to merge. (c') The six paired minima merged in three shallow minima.

The condition $C > \beta^2/4\gamma$ must be satisfied to keep the free energy positive at large Q .

We notice from Eq. (4) that η and β term are of the same order in Q and can compete with each other. A critical value $\eta_c = -\beta^2/4\gamma$ defines two cases in which either the sine or cosine term dominates in the free energy. Fig. 2 shows how the structure of the minima changes in the two cases. Supplementary Figures S1 and S2 show in greater detail how the free energy density changes with the parameters α and η .

To simplify the analysis we redefine F by dividing by the coefficient of the cosine term

$$F = (\eta + 1)Q^6 \sin^2 3\phi + \alpha Q^3 \sin 3\phi - AQ^2 - BQ^4 + CQ^6, \quad (5)$$

where all the coefficients in the equation have been adequately rescaled and $\eta_c = -1$. We show in Fig. 3 the free energy density from Eq. (5) and the polarization P_z from Eq. (3) for different values of α and in the two cases $\eta > \eta_c$ and $\eta < \eta_c$.

We now discuss the role of α and η terms. The term $\alpha Q^3 \sin 3\phi$ has three minima while the terms $Q^6 \cos^2 3\phi$ and $\eta Q^6 \sin^2 3\phi$ have six minima. As we vary α , the total number of minima in the free energy changes. Small values of α will favor the 6th-order terms and the free energy will have six minima (Fig. 2 (a,b) and (a'b')). As $|\alpha|$ grows the $\alpha Q^3 \sin 3\phi$ term dominates over the 6th-order terms forcing the free energy into a three-minima configuration. A change of sign in α produces a 60° rotation of the minima of the free energy (cf. supplementary

figures S1 and S2). The coefficient η controls the competition between the $-Q^6 \cos^2 3\phi$ term and the $\eta Q^6 \sin^2 3\phi$ term and selects the position of the free energy minima in the low- α range (cf. Fig. 2(a,a')). The η coefficient selects the cases where a finite polarization can be present in the material. Figure 3 (a'-d') shows the polarization P_z (in orange) computed with Eq. (3) as a function of the angle ϕ and the corresponding value of the free energy (blue) for a fixed Q and the same angle. We see that, if $\eta > \eta_c$ and for small values of α , the polarization has a finite value at the minima of the free energy. On the other side, if $\eta < \eta_c$ the polarization is always zero at the free energy minima, that correspond to the structural domains. Although the polarization P_z is zero at the minima, it has non-zero values in the domain walls, across which \mathbf{Q} interpolates between the neighboring minima. To summarize, in the case $\eta > \eta_c$, the system exhibits ferroelectric domains, while for $\eta < \eta_c$ it has ferroelectric domain walls.

Inner structure of domain walls – The minima of the free energy represent the possible orientation of DMA molecules. At small α all the barriers along the rim of the Mexican hat have the same height, and the six minima are energetically equivalent.

Six domains with different \mathbf{Q} orientations are possible and, when the domains meet at the same line (vortex line), an hexagonal vortex defect is formed [14]. A cut perpendicular to the vortex line is shown in Fig. 6 (d, top right). Figure 6 shows a schematic phase diagram of our model in the $[\eta, \alpha]$ space. When moving along the α axis, at $|\alpha| > \alpha_c$, we obtain a phase with three minima, corresponding to three possible domains separated by domain walls.

The inner structure of domain walls here is connected to three of the six minima going up in energy, thus making the corresponding states metastable. Once we discuss the domain walls, *i.e.* configurations with spatially varying order parameter, we must complement our free energy density from Eq. (5)

$$F_{\text{tot}} = \int dr \left(\frac{m}{2} [(\nabla Q_x)^2 + (\nabla Q_y)^2] + F(Q) \right), \quad (6)$$

with the first term being the stiffness term that penalizes order parameter variations. Then the problem of describing the structure of the domain walls, *i.e.* minimizing Eq. 6 is equivalent to the problem of determining the trajectory $Q(r)$ (with $\phi = \phi(r)$) of a classical particle in a flipped potential $\mathcal{V} = -F$, *i.e.* minimizing the Lagrangian $m/2 \dot{x}^2 - \mathcal{V}$. In the case $\eta < \eta_c$ the minima that are less shallow in the free energy (cf. Fig. 2(b)) are maxima of lower height in the classical analogue (Fig. 4(a)). The particle starts at the top of the potential (minimum of the free energy) with zero velocity and it passes the neighboring peak (local minimum higher in energy) with a non zero velocity, spending a finite amount of time near the peak. This second peak represents an “unfavored do-

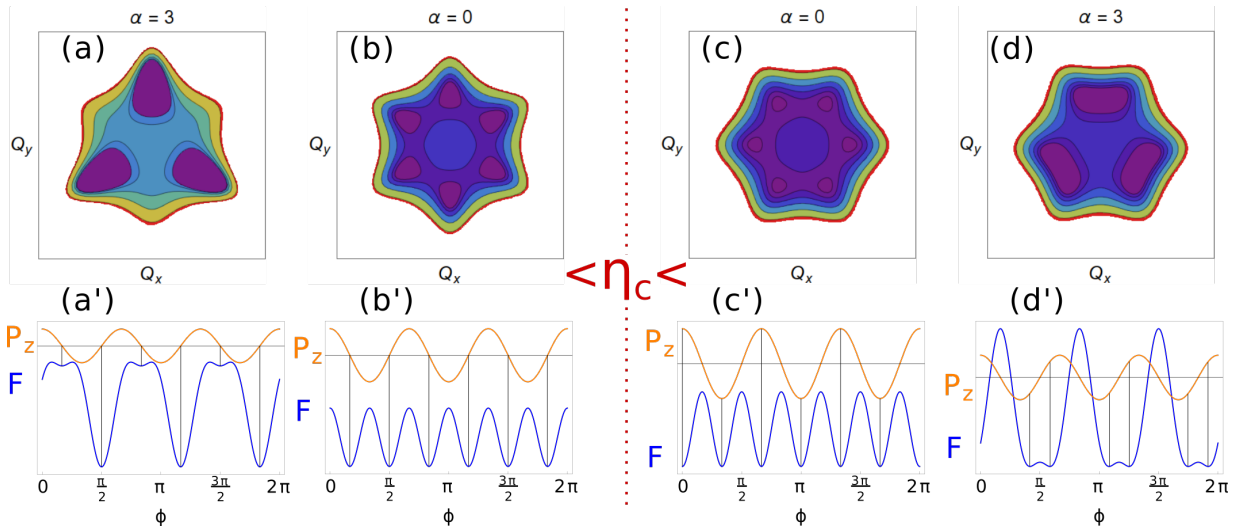


FIG. 3. (a-d) Free energy density for different values of α and η . (a'-b') polarization profile and free energy as a function of the angle ϕ for different values of α and η . In $\eta < \eta_c$ (left) the polarization is zero in correspondence of the minima of the free energy. Solid lines in (a',b') connect the minima of F to the corresponding value of P_z . In $\eta > \eta_c$ the polarization is non zero at the minima of the free energy, it has the maximum value (in modulus) at $\alpha = 0$ and decreases with growing $|\alpha|$.

main" inside a domain wall. The time that the particles spends at the smaller peak is proportional to the finite width of this inner domain.

Domain walls with inner structure, or *nested domain walls*, are not commonly observed, therefore the properties of these objects have not yet been characterized. This in turns, clearly suggests a rich phase diagram of these complex hybrid materials, including the possibility of electric skyrmions,[15] therefore calling for further experimental and theoretical investigations. The phase diagram in Fig. 6 helps identify the phases where such nested domains walls are expected. Fig. 5 shows, for different values of α , the presence of inner structure in the domain walls.

In the case $\eta > \eta_c$ all minima of the free energy are equally deep thus, in the classical analogue, all the peaks

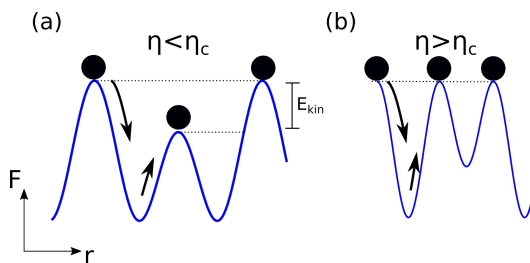


FIG. 4. Classical particle in a flipped free energy potential (blue curve) in the case $\eta < \eta_c$ (a) and $\eta > \eta_c$ (b). (a) on top of the lower hill the particle has lower kinetic energy than in the minimum and it spends a greater amount of time there. Equivalently, Q stays in a metastable state, which results in the inner structure of the domain wall. (b) all hills have the same height and no metastable state is present.

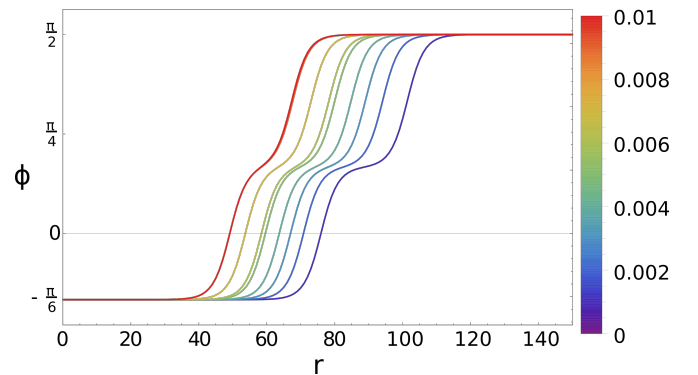


FIG. 5. Spatial profile of nested domain walls. The trimerization angle profile $\phi(r)$ represents the structure of the wall, and the inner structure, corresponding to a metastable phase, is present between the two domains, identified by ϕ values of $\pi/2$ and $-\pi/6$. The domain wall profile is computed for different values of α , which are encoded by the color. The length scale on the horizontal axis (arb. units) is set by the order parameter stiffness, represented by the parameter m in the free energy.

have the same height and no internal structure is expected (cf. Fig. 4(b)). In the supplementary Figure S3 we report the trajectories Q computed for both $\eta > \eta_c$ and $\eta < \eta_c$. In summary, as discussed above, several regimes are possible within the presented theory, such as ferroelectric domains and non-ferroelectric domains with ferroelectric domain walls. Accurate density functional theory calculations for different compounds will allow to estimate the model parameters and position the materials on the phase diagram (cf. Fig. 6).

Conclusions – In this study we built a Landau the-

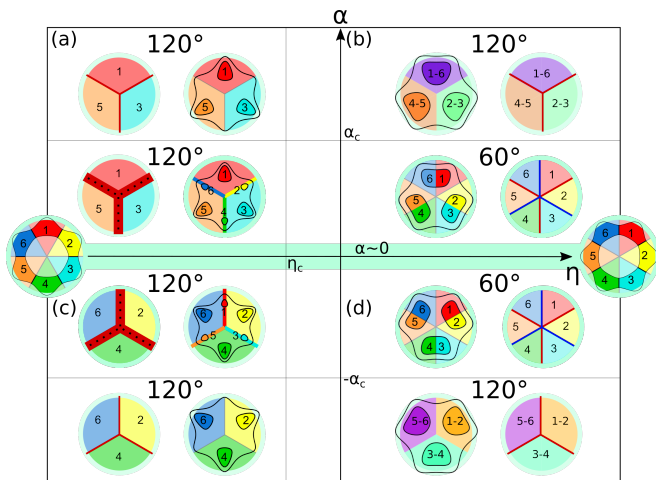


FIG. 6. Summarized phase diagram in the parameter space $[\eta, \alpha]$ computed with the free energy from Eq. (5). At $\alpha = 0$ six equivalent minima give rise to 6-fold vortices, shown at the endpoints of the horizontal η axis. The phase diagram shows a schematic profile of the energy density (with contours in black) for every phase in the parameter space $[\eta, \alpha]$ and the corresponding structure of domain walls and vortices. The value η_c separates two regimes where six-minima turn into three with different mechanisms. The value $|\alpha_c|$ selects the threshold on the α axis, after which there are only three minima in the free energy and no internal structure is present in the domain walls.

ory of phase transition describing the molecular ordering and ferroelectric polarization in MOFs, in particular in the perovskite-based hybrid inorganic-organic (DMA)Fe^{II-III}(COOH)₃. The results suggest that ferroelectricity can arise from tripling of the unit cell due to molecular ordering. Wide composite domain walls, with the metastable states realized inside the domain walls, are predicted. We find vortex line defects, where three of six domain walls merge. Our study highlights the complex and rich phase diagram due to the interplay of molecular and framework degrees of freedoms thanks to the dual nature of MOFs. We hope the our work will motivate experimental and *ab-initio* investigations of this

mechanism which may be more generally found in MOFs.

-
- [1] P. Jain, A. Stroppa, D. Nabok, A. Marino, A. Rubano, D. Paparo, M. Matsubara, H. Nakotte, M. Fiebig, S. Picozzi, E. S. Choi, A. K. Cheetham, C. Draxl, N. S. Dalal, and V. S. Zapf, NPJ Quantum Materials **1**, 16012 (2016).
 - [2] H. Li, H.-B. Liu, X.-M. Tao, J. Su, P.-F. Ning, X.-F. Xu, Y. Zhou, W. Gu, and X. Liu, Dalton Transactions **47**, 8427 (2018).
 - [3] S. Horiuchi and Y. Tokura, Nat Mater **7**, 357 (2008).
 - [4] P. S. Ghosh, D. DeTellem, J. Ren, S. Witanachchi, S. Ma, S. Lisenkov, and I. Ponomareva, Phys. Rev. Lett. **128**, 077601 (2022).
 - [5] J. Li, Y. Liu, Y. Zhang, H. L. Cai, and R. G. Xiong, Phys Chem Chem Phys **15**, 20786 (2013).
 - [6] L. C. Gómez-Aguirre, B. Pato-Doldán, J. Mira, S. Castro-García, M. A. Señaris-Rodríguez, M. Sánchez-Andújar, J. Singleton, and V. S. Zapf, Journal of the American Chemical Society **138**, 1122 (2016).
 - [7] G. Long, R. Sabatini, M. I. Saidaminov, G. Lakhwani, A. Rasmita, X. Liu, E. H. Sargent, and W. Gao, Nature Reviews Materials **5**, 423 (2020).
 - [8] G. Tang, W. Ren, J. Hong, and A. Stroppa, The Journal of Chemical Physics **151**, 124704 (2019), <https://doi.org/10.1063/1.5116343>.
 - [9] J. Guo, L. Chen, D. Li, H. Zhao, X. Dong, L. Long, R. Huang, and L. Zheng, Applied Physics Letters **110**, 192902 (2017), <https://doi.org/10.1063/1.4983169>.
 - [10] L. Cañadillas-Delgado, O. Fabelo, J. A. Rodríguez-Velamazán, M.-H. Lemée-Cailleau, S. A. Mason, E. Pardo, F. Lloret, J.-P. Zhao, X.-H. Bu, V. Simonet, C. V. Colin, and J. Rodríguez-Carvajal, Journal of the American Chemical Society **134**, 19772 (2012).
 - [11] C. Capillas, E. S. Tasci, G. de la Flor, D. Orobengoa, J. M. Perez-Mato, and M. I. Aroyo, Zeitschrift für Kristallographie - Crystalline Materials **226**, 186 (01 Feb. 2011).
 - [12] H. T. Stokes, D. M. Hatch, and C. B. J., “Isodistort, isotropy software suite,” iso.byu.edu.
 - [13] B. J. Campbell, H. T. Stokes, D. E. Tanner, and D. M. Hatch, Journal of Applied Crystallography **39**, 607 (2006).
 - [14] S. Artyukhin, K. T. Delaney, N. A. Spaldin, and M. Mostovoy, Nat Mater **13**, 42 (2014).
 - [15] H. L. Bostrom and A. L. Goodwin, Accounts of Chemical Research **54**, 1288 (2021).

SUPPLEMENTARY INFORMATION

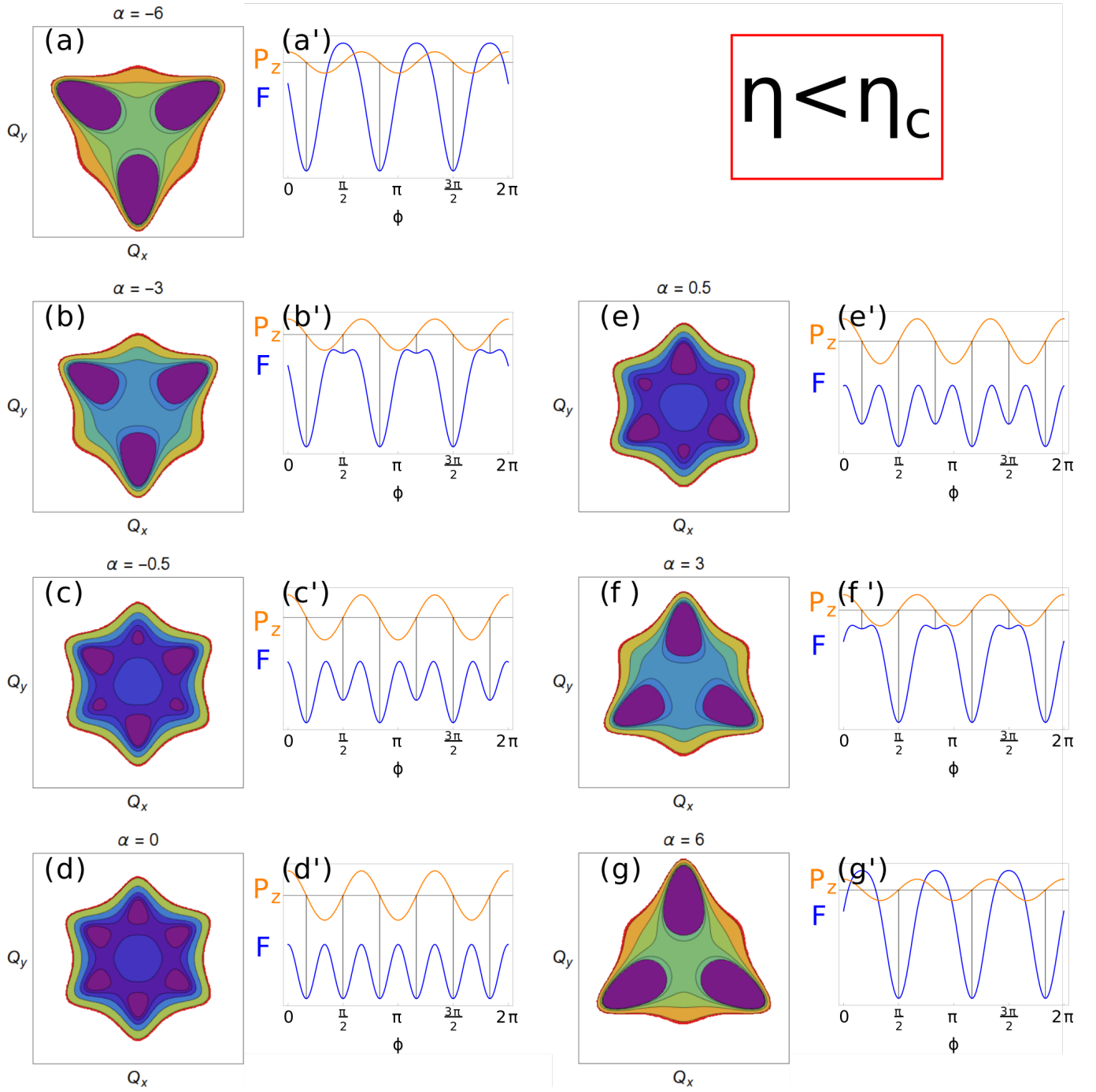


FIG. S1. (a-e) Free energy surface in the case $\eta < \eta_c$ for different values of α . (a'-e') Free energy F and polarization P_z as a function of the angle ϕ . Solid lines are a guide to the eye. In correspondence of the minima of F the polarization is zero for all values of α . When α changes sign the position of the minima is rotated by 60° .

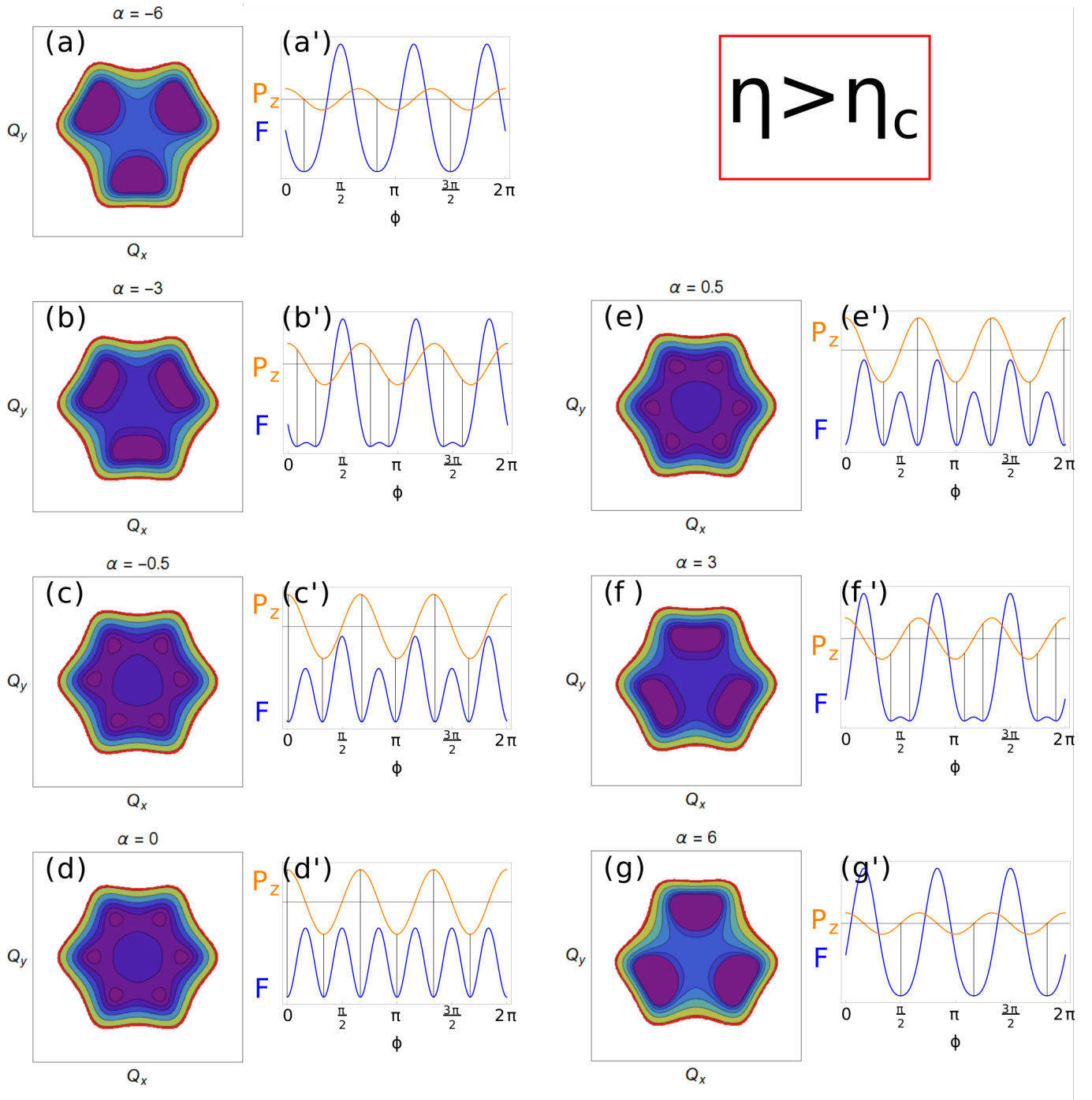


FIG. S2. (a-e) Free energy surface in the case $\eta > \eta_c$ for different values of α . (a'-e') Free energy F and polarization P_z as a function of the angle ϕ . Solid lines are a guide to the eye. In correspondence of the minima of F the polarization is non-zero for small values of α . When α changes sign the position of the minima is rotated by 60° .

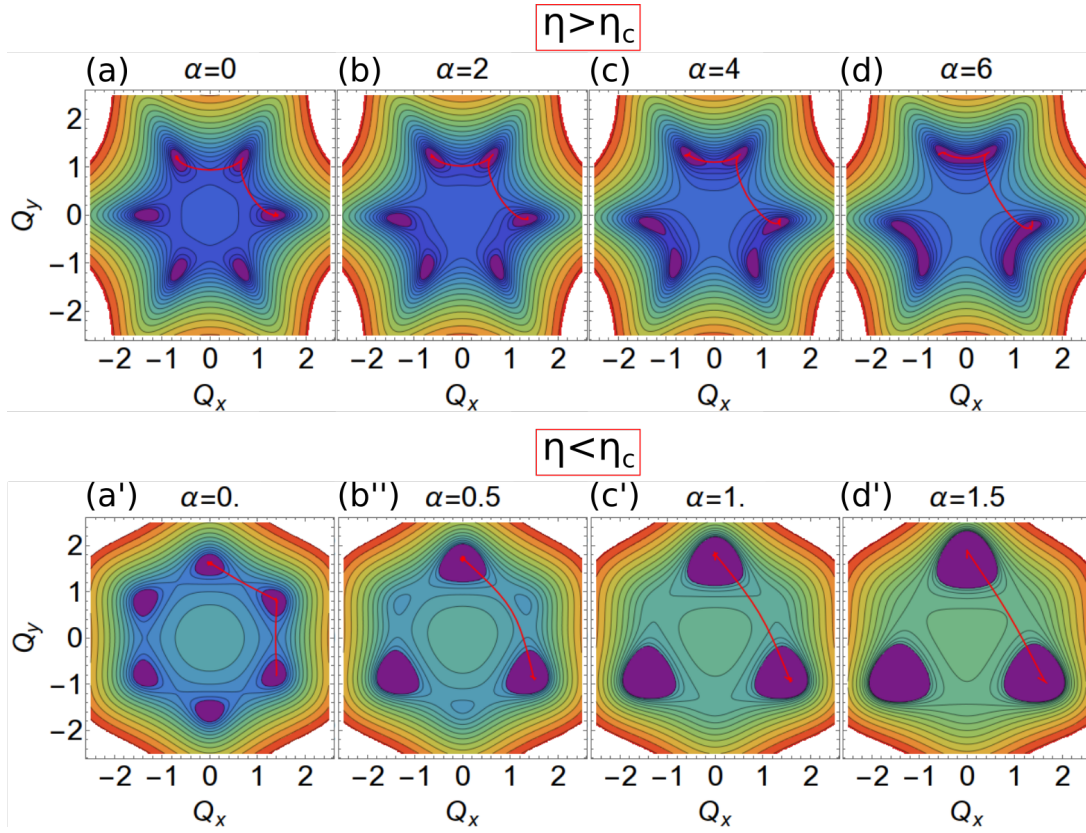


FIG. S3. Computed trajectories in the classical problem with flipped potential $\mathcal{V} = -F$, from a minimum to the equivalent one defined by a rotation of 120° degrees. (a-d) $\eta > \eta_c$ case, the transition from 6 to three minima happen by merging of two adjacent minima. The trajectory of the particle always visits all the three minima as they are all of the same energy. (a'-d') $\eta < \eta_c$ case, three unfavored minima turn into maxima. The classical particle visit the minima in $\alpha = 0$ but the trajectory gets farther from that point as the minimum becomes a maximum.